Threshold-based 5G NR base station management for energy saving

Computer Networks 259 (2025) 111070

Contents lists available at ScienceDirect

Computer Networks

journal homepage: www.elsevier.com/locate/comnet

Threshold-based 5G NR base station management for energy saving

Greta Vallero [a,*], Michela Meo [a], Wout Joseph [b], Margot Deruyck [b]

[a] Politecnico di Torino, Department of Electronics and Telecommunications, C.so Duca degli Abruzzi 24, 10129 Torino, Italy
[b] Ghent University, IMEC–WAVES, Technologiepark–Zwijnaarde 126, 9052 Ghent, Belgium

ARTICLE INFO

Keywords:
Radio access network
Base station
Sleep mode
Energy saving

ABSTRACT

In spite of promising outcomes in optimizing energy usage for Radio Access Network (RAN) Base Station (BS) hardware, deployment, and resource management, existing methods frequently lack flexibility for scenarios involving multiple frequencies and technologies of BSs. This investigation presents a comprehensive BS switching strategy based on a threshold, tailored for real-world multi-frequency and multi-technology BSs within the RAN. The proposed approach strategically deactivates BSs using a threshold parameter that determines the maximum allowable growth in transmission power for active BSs, ensuring both coverage for users affected by BS deactivation and energy saving. Simulations conducted on a realistic multi-technology 5G New Radio (NR) RAN in an urban environment validate the efficacy of the proposed strategy, achieving up to 73% of energy saving. The study assesses the influence of the frequency order of BS deactivation and examines user re-association strategies aimed at minimizing either path loss or transmission power.

1. Introduction

Wireless technology is envisioned to play a pivotal role in reducing greenhouse gas (GHG) emissions across various sectors of society. This is realized through providing connectivity for digital solutions that aim to curtail energy consumption, minimize travel and transportation, and generally mitigate GHG emissions [1]. Examples of such applications include providing connectivity for buildings to facilitate energy management and supporting vehicle communication to reduce fuel consumption and optimize routing. In addition to the more traditional aspects of remote and mobile working that contribute to emission reduction from travel, areas such as agriculture, health, the sharing economy, and smart cities held significant potential for future reductions in emissions [1–3]. The impact of mobile-based solutions is closely related to improvements in connectivity, making operators' networks scalable, secure, and standardized means to connect assets across various services in an economically sustainable manner. Nevertheless, these services and application further contribute to the growth of the data traffic managed by the wireless network and because of this, to the rise in its energy consumption. Wireless systems and networks are significant consumers of resources, encompassing both electricity and raw materials. The energy demand for operating these networks is substantial: according to [4], in 2020, China's mobile networks and data centers alone consumed approximately 201 TWh of energy, that corresponds to around 2.3% of the nation's total energy consumption. With the ongoing deployment of 5G networks, the growth of consumer demand and the trend towards utilizing data centers for virtualized mobile networks, a 289% growth in energy use by wireless networks in China between 2020 and 2035 is forecast [4]. As reported by [2], although the edge network, data centers, and core services individually contribute to no more than 25% of the energy consumption by network operators, the RAN alone constitutes 73% of this total. Beside this, since most of the energy that we use nowadays comes from burning fossil fuels, addressing this rise of energy demand is crucial for the sustainability of future networks. This is also to respond to the Sustainable Development Goals and the Paris Agreement on Climate Change that recommend that countries reduce carbon emissions by 45% by 2030 and to net zero by 2050 [5]. Efforts to diminish energy consumption in RAN have garnered significant attention in the research community, resulting in promising outcomes [6,7]. Studies typically seek to optimize various aspects, such as the BS hardware components design [8,9], the deployment positioning of BSs [10], radio transmission mechanisms [11], BS switching [12], and local energy harvesting enhancements [13]. BS switching in a RAN entails activating and deactivating various BSs within the network. This process enhances the unevenly distributed traffic demand across a mobile network. Typically, 50%–70% of BS sites handle only 25% of the total traffic [14]. These low-load sites are frequently over-dimensioned, operating at suboptimal capacity utilization levels, resulting in unnecessary high energy consumption. In [15], authors introduce a deep Reinforcement Learning (RL) approach for energy consumption reduction, that integrates

* Corresponding author.
E-mail address: greta.vallero@polito.it (G. Vallero).

https://doi.org/10.1016/j.comnet.2025.111070
Received 23 January 2024; Received in revised form 14 October 2024; Accepted 15 January 2025
Available online 29 January 2025

energy consumption, IP throughput rate, and handover considerations into the reward function. In [16], a Graph Neural Network (GNN) represents the network topology as a graph, where each BS acts as a node and incorporates traffic conditions as node features. This method involves learning an embedding vector for each node, which is then used to determine on/off switching decisions, for energy optimization.

The existing literature highlights that BS switching emerges as a promising solution to mitigate RAN power requirements. However, it is noteworthy that these approaches are often specifically designed for scenarios involving single-frequency and single-technology BSs. Nevertheless, BSs that implement different technologies or operate on different frequencies provide varying levels of Quality of Service (e.g., coverage, available bandwidth, and maximum supported users) and exhibit different power consumption behaviors. This means that deactivating a BS using one technology or frequency may have a different impact on network power usage compared to deactivating another BS using a different technology or frequency. In addition, works in the current literature usually depend on predefined performance degradation constraints that might overlook real-time changes in traffic. In this paper, we overcome these limitations and we present a solution that takes into account multi-frequency (800 MHz, 2100 MHz, and 3500 MHz) and multi-technology (beamforming and omnidirectional) BSs within the RAN. This involves formulating and implementing a BS switching policy that is strategically designed based on the unique power requirement characteristics exhibited by the BSs. We evaluate our proposal through simulations on a realistic RAN covering the city of Zurich, Switzerland. The contributions of this work are the following:

- Proposing a BS switching strategy aimed at reducing RAN power requirements. This strategy deactivates a BS if its users can be covered by active BSs and if the growth of transmission power needed for covering those users is lower than a threshold ρ^*. Using the power need model of each BS technology, we formalize and generalize the formulation of the threshold ρ^* to ensure energy savings.
- After an overview of the power need models of 5G New Radio (NR) BSs operating at different frequencies, as well as Massive Multiple Input Multiple Output (MA-MIMO) BSs, we quantify the value of the threshold ρ^*. It is the maximum allowable transmission power growth to cover users who remain uncovered due to BS deactivation. This quantification is presented in terms of transmitted watts and translated to meters to measure the allowable increase in coverage radius of active BSs, considering different transmission power levels for both the deactivated BS and the active ones, in both Line of Sight and No Line of Sight (NLoS) cases.
- Conducting simulations to evaluate and quantify the impact of the frequency order of BS deactivation and implementing two different approaches for the re-association of users when a BS is deactivated, aiming to minimize either the experienced path loss or the transmission power. Results show that using a re-association based on path loss slightly reduces power requirements compared to when re-association minimizes transmission power.

The paper is organized as follows: Section 2 reviews related works, Section 3 provides an overview of power requirement models for BSs of different technologies, Section 4 presents the scenario and our proposed methodology, and Section 5 describes the Key Performance Indicators (KPIs) used. Section 6 formulates and quantifies the values of the threshold ρ^* on which our switching approach is based. Results are discussed in Section 7, and our findings are drawn in Section 8. Section 9 concludes our work.

2. State of the art

As mentioned in the previous section, a lot of efforts have been done towards energy efficient RAN [1–3]. This is because this aspect is now acknowledged by network operators as a pivotal criterion for the forthcoming decade in the RAN. This recognition is grounded in the dual advantages of diminishing operational (OPEX) costs and increasing the sustainability of network systems. Enhancing the energy usage of the network not only results in cost reductions for operators and sustainability, but also facilitate the progress of communication technology in developing countries [17]. The proposed solutions encompass a spectrum of strategies that can be classified into five key categories, each targeting specific aspects of network operations. These categories include the optimization of BS hardware components, the implementation of sleep mode strategies, enhancements in radio transmission mechanisms, meticulous network deployment and planning, and the integration of energy harvesting technologies [8–13]. Among these categories, sleep mode strategies have emerged prominently in the focus of various studies in the literature. These strategies involve optimizing the operational states of network elements during periods of low demand, contributing significantly to overall energy efficiency. Indeed, RANs are usually planned and deployed to meet certain peak-hour requirements, which leads to an overdimensioning of the network for the less challenging traffic loads during the day time [18]. As the traffic demands fluctuates over both time and space, underutilized BS resources could be dynamically switched off to save energy. The more network components that are shutdown and the longer the time that they are shutdown, the more energy can be saved. This heightened interest is particularly accentuated in the context of 5G and 6G networks, where the aspect of network energy-efficiency is a priority.

In [19], Piovesan et al. contemplate a hierarchical arrangement wherein a subset of its BSs relies solely on solar panels and batteries for the power supply. These BSs are organized into clusters and linked within a micro-grid framework. A central controller manages BSs sleep mode and the energy distribution across them, leveraging Machine Learning models to access the optimal sleep mode and energy distribution policies. Similarly, the study outlined in [20] aims at achieving energy efficiency through the implementation of BS sleep mode. In order to do this, authors employ a reinforcement learning approach to intelligently and dynamically learn effective strategies for user-equipment association and orthogonal frequency-division multiple access scheduling. The authors in [21] introduce a time-varied probabilistic ON/OFF switching algorithm designed for application in cellular networks. Additionally, the work presented in [22] propose an algorithm for throughput and energy efficiency enhancement in 5G dense RAN. The proposed algorithm uses a deep neural network, to take decision to put the BSs into a sleep mode and the transferable payoff coalitional game theory is used to give to real-time applications a higher priority over non-real time applications. Authors in [23] develop a grid-connected solar panel power supply system for traffic-aware RAN. The goal of this work is to minimize grid energy consumption, introducing a load balancing technique among BSs to optimize resource block utilization. Furthermore, in [24,25], RoD strategies are implemented within a green mobile access network to enhance its interaction with the smart grid within a demand response framework. The aim is to reduce electricity costs and provide ancillary services. Differently, the implementation of the sleep mode in [26] is used to regulate the resource and power requirement in small cell Orthogonal Frequency-Division Multiple access (OFDMA) networks. With the support of weighted graph theory, work in [27] employs a dynamic structural algorithm for the control of the activation/deactivation of BSs in RANs without compromising the user coverage, by managing the network's load through coordination with neighboring cells.

Closely related to this paper are our previous works in [28–33] In [28,29], we present a deployment tool based on capacity considerations for designing energy-efficient wireless access networks, that

Table 1
Link budget parameters for the different BSs [34–37].

Parameter	800 MHz	2100 MHz	5G 3500
Frequency (MHz)	800	2100	3500
Bandwidth (MHz)	120	120	120
Used Subcarriers	7680	7680	7680
Total Used Subcarriers	12 288	12 288	12 288
Sampling Factor	1536	1536	1536
TDD Duty Cycle DL (%)	75	75	75
TDD Duty Cycle UL (%)	25	25	25
Spatial Duty Cycle (%)	0	0	15
BS Transmit Antenna Gain (dBi)	16	18	24
BS Transmit Array Antenna Feed Loss (dBi)	2	2	3
BS Radiated Power (dBm)	46	49	53
BS Number of Antenna Elements	1	1	64
User Antenna Element Gain (dBi)	0	0	0
User Transmit Power (dBm)	23	23	23
User Antenna Height (m)	1.5	1.5	1.5
User Number of Antenna Elements	1	1	1
RX Noise Figure (dB)	8	8	7

Table 2
Power requirement model parameters [34].

Parameters	Explanation	Values
P_T (W)	Radio frequency transceiver power	1.5
η	Efficiency of the power amplifier	0.5
P_B (W)	BH power link	10
P_C (W)	Cooling system power	200
P_R (W)	Rectifier power	50
P_{DSP} (W)	Digital signal processing power	1
N_A	Number of antenna sectors	1 for 800 MHz, 2100 MHz BS 64 for 3500 MHz BS

adapts the RAN capacity to meet instantaneous traffic demand. Additionally, our work introduces supplementary sleep mode intervals for BSs during renewable energy generation shortages. The study in [30] compares the effectiveness of various energy-aware strategies, incorporating BS sleep modes, while balancing the reduction in on-grid energy demand against the provided network capacity. Analytical models are formalized to forecast the performance of the green network concerning solar panel size and storage capacity, used for the BS supply. In [31], we leverage Machine Learning predictions to evaluate future traffic demand and renewable energy sources production. We then dynamically manage RAN resources based on these predictions to minimize the energy consumption and drawn from the power grid. In [32,33], we analyzes the effect of the caching feature of the Multi-Acces Edge Computing (MEC) paradigm on the micro cell BSs sleep mode employment and we design user association policies, to totally exploit the MEC technology and reduce the network energy consumption.

While these works introduce promising strategies for BS switching, they do not consider the heterogeneity of BSs in terms of frequency and technology. To the best of our knowledge, no existing studies have developed BS switching policies that consider multi-frequency and multi-technology BSs. BSs operating at different frequencies or technologies provide varying coverage, bandwidth, maximum supported users, and power requirements. Consequently, deactivating BSs with different technologies and/or frequencies can have differing impacts on network power usage.

To address this limitation, we propose a solution that considers a real multi-frequency and multi-technology BS RAN and we develop a BS switching policy based on the power requirement characteristics of the BSs.

3. Power requirement in RAN

Before going into the details of our proposed methodology, we briefly discuss in this section, the characteristic of the considered BSs and their power requirements.

As widely recognized, 5G NR represents the latest standard in the evolution of next-generation networks, marking a significant shift towards a user and application-centric technology framework [38]. Our focus in this study is on the Enhanced Mobile Broadband (eMBB), one of the three pivotal use cases supported by 5G, alongside Machine Type Communications (mMTC) and Ultra-reliable Low Latency Communications (ULLC). The adoption of 5G NR Release 14 introduces the use of Massive Multiple Input Multiple Output (MaMIMO), an advanced antenna array system with hundreds of antenna elements, significantly increasing throughput [39]. In contrast to the traditional 4G approach, where BSs consist of three sectors covering 120 degrees, MaMIMO is often coupled with beamforming, which consolidates all data and signaling towards the user, positively impacting the link budget, reducing interference, and providing higher data rates. For our simulations, we use a RAN where a portion of its BSs employs MaMIMO technology at a frequency of 3500 MHz, using beamforming as the steering technique. The remaining BSs in the network use omnidirectional antennas and exclusively support 5G NR on the 800 MHz and 2100 MHz frequency bands, the same frequencies used by the 4G technology. Table 1 illustrates the link budget for 5G NR technology across various frequencies, based on [34–37]. As mentioned in previous sections, in this work, we design a BS switching approach suited for a multi-frequency (800 MHz, 2100 MHz, and 3500 MHz) and multi-technology (beamforming and omnidirectional) scenario. For the remainder of the paper, we refer to each BS type by its frequency band, without explicitly mentioning the steering technique used.

In this part of the work, we discuss the models that formalize the power needs of the BSs, integrated into the simulation framework used for evaluating our proposed methodology. Literature highlights that BSs in the RAN constitute the most energy-intensive segment, accounting for 73% of the network's overall energy requirements, surpassing the energy needs of the edge network, data centers, and core services [2, 40]. The primary goal is to provide a comprehensive understanding of the dynamics of power requirements within 5G wireless networks.

In the literature, several models quantify the power requirements of a BS, typically depending on transmission power or BS load. The EARTH project, in [41], formalized two distinct models based on measurements of Long Term Evolution (LTE) equipment. The first model

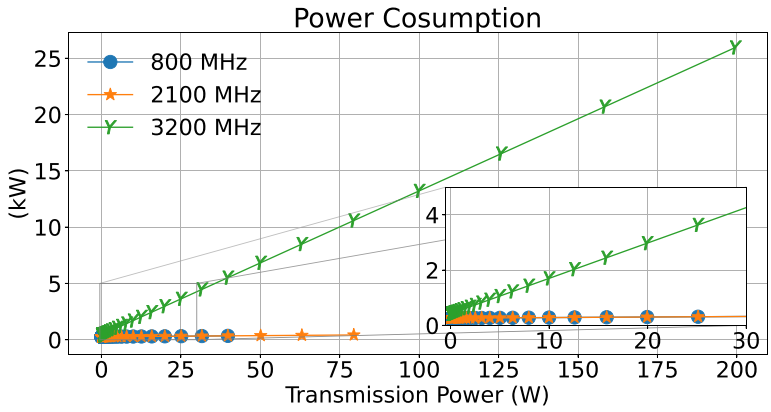

Fig. 1. Power requirements for the different BS technologies.

estimates the BS power consumption at maximum load, and the power requirement linearly grows with the number of transceiver chains; while the second relates BS power usage linearly to the number of utilized resource blocks. Similarly, the model discussed in [42] defines the power requirements of a 4G BS as load-dependent. In [43], the authors propose a model for 4G BS power usage that is linearly proportional to transmission power, validated through real measurements. In line with these models, the authors in [43–45] formalize the power requirements of a 5G BS as linearly dependent on transmission power. Given that it accounts for 5G-specific features such as beamforming, we choose this model for our work.

Similar to the EARTH model formalized for LTE technology in [41], the 5G BS comprises six key power-consuming components:

- *Digital Signal Processing* (DSP) — Responsible for the digitization and processing of the analog signal.
- *Power Amplifier* — It converts DC input power into the radio frequency signal.
- *Air Conditioning* — This maintains the optimal temperature for seamless BS equipment operation.
- *Backhaul Link* — It is used for the communication between the backhaul network and the BS, utilizing either a microwave or fiber link.
- *RF Transceiver* — It facilitates the signal transmission and reception at the BS.
- *Rectifier* — This converts AC to DC, essential for BS equipment operation.

According to [44–46], these power contributions are formalized in the total BS power requirements as:

$$P_c^{(t)} = N_A \left(P_T + P_{DSP} + \frac{P}{\eta} \right) + P_R + P_C + P_B \tag{1}$$

where N_A is the number of elements of the BS antenna (see Table 1), P_T is the power of the radio frequency transceiver, in W, P_{DSP} is the power of the digital signal processing, in W, η is the efficiency of the power amplifier, and P is its transmitted power, in W. P_R, P_C, and P_B are the power drained by the rectifier, the cooling system, and the backhaul link, respectively, in W. Refer to Table 2 for the values of the parameters [46]. According to the model, the air conditioning and backhaul power are constant, while the power consumed by the BS equipment components (DSP, power amplifier, and RF transceiver) scales with the number of antenna elements. To estimate the total power withdrawn by these components, their respective power values are multiplied by the number of antennas.

Fig. 1 illustrates the total power requirements, in kW, for different BSs, utilizing frequencies of 800 MHz, 2100 MHz, and 3500 MHz, denoted by blue, orange, and green lines, respectively, while varying the transmission power, in W on the x-axis. It is evident from the figure that BSs operating at 800 MHz and 2100 MHz do not exceed 0.45 kW in power requirements. In contrast, the 3500 MHz BS demands up to 26 kW, which is up to 98% more than the maximum power needs of the 800 MHz and 2100 MHz BSs. This substantial difference is attributed to the larger transmission power levels that the 3500 MHz BS can reach. Moreover, even when operating at the same power transmission level, it consistently requires more power than the 800 MHz and 2100 MHz BSs, as shown in the zoomed-in view of the inner plot in Fig. 1, because of its large number of antennas elements (see Table 2).

4. Evaluation framework

In this work, we extend the framework of [10] to our methodology, as explained below. The tool in [10] designs an optimized RAN, towards human exposure. Its output is the position of the BSs, which minimize the electromagnetic exposure. As in that work, we consider the urban area of Zurich, in Switzerland. According to the map provided by [47], the area is 70.4 km^2, resulting in a population density of 5897 people/km^2, based on the population reported in [48]. The link budget parameters are as in [10] and summarized in Table 1. As in [28], we run 30 simulations to obtain a good estimation of the results and we compute mean and confidence interval of the relevant KPIs.

4.1. Input

As in [10], our simulator framework requires several inputs. First, the shape file contains detailed 3D information about the buildings in Zurich, Switzerland (see Fig. 3). The positions of the BSs are obtained from [10], as depicted in Fig. 3, comprising a total of 285 BSs. As mentioned above, in 5G NR Release 14, the use of advanced antenna arrays, known as MaMIMO, is enabled. It incorporates hundreds of antenna elements to significantly boost throughput, positively influencing the link budget and reducing interference, resulting in higher data rates [49].

For our simulations, we assumed that part of the BSs in a 5G network would utilize MaMIMO technology at a frequency of 3,500 MHz. All other BSs in the network support only 5G NR on the 800 MHz and 2100 MHz frequency bands. They account for 105, 102 and 78 BSs, respectively. Tables 1 presents the network parameters and receiver sensitivities for 5G NR technology.

Next, we provide the number of users in the simulated scenario (see Fig. 3). The number of users aligns with data collected by operators in 2020. At peak times, there are 1898 simultaneous active users, according to data confidentially provided by operators. To account for

Fig. 2. Map of the simulated region, delimited by the area in orange, covering 70.4 km^2, in the urban area of Zurich, in Switzerland.

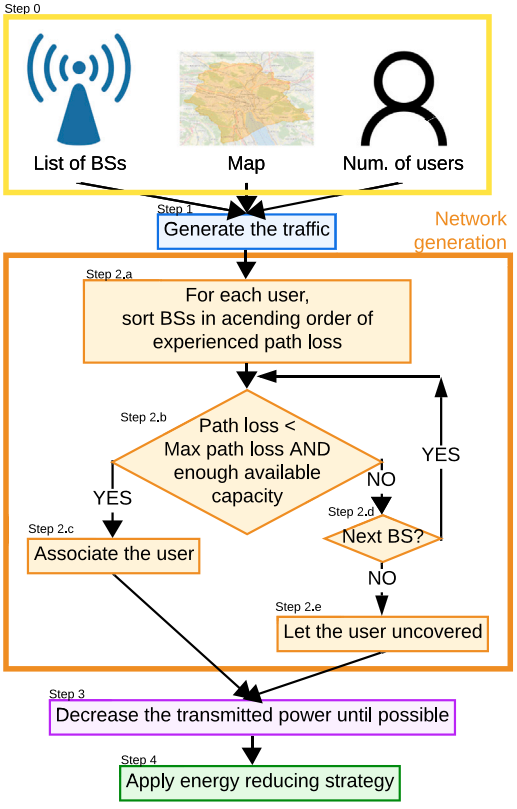

Fig. 3. Flow chart with the different steps of our simulations.

traffic growth between 2021 and 2030, we consider a compound annual growth rate of 2.2%, which results in a total of 9595 users [50]. Finally, to determine the number of users for a specific operator, we use data from the Swiss Market Distribution, indicating that for the considered operator, the share is 15.31%. Consequently, the number of users is set at 2466.

4.2. Traffic generation

The simulator initiates traffic generation (depicted by the blue rectangle in Fig. 3). For each user u, we determine the 3D coordinates $(x^{(u)}, y^{(u)}, z^{(u)})$, located inside the orange area in Fig. 2. These coordinates are generated uniformly, considering the absence of hotspots like tourist attractions or parks, ensuring an equal chance for each location. In addition to the position, the requested bit rate is set to 10 Mbps [10,34].

4.3. Generation of the network

After traffic generation, the association process initiates (depicted by the orange rectangle in Fig. 3), and each user is linked with the BS that yields the lowest path loss. For each user, a list of potential BSs is created, and a BS is included in the list if it can provide the required bit rate and the experienced path loss is below a permissible maximum. The selected BS is the one that results in the user experiencing the lowest path loss. If the list is empty, meaning no BS is able to provide the required bit rate and a signal of adequate quality, the user remains without coverage, as in a real-world scenario.

To determine the experienced path loss, the direct line between the user and each considered BS is established. Accounting for the presence of existing buildings, whose 3D data are provided as input to the framework, we ascertain whether the user is in Line-of-Sight (LoS) and Non-Line-of-Sight (NLoS). In line with the directives by the mobile broadband standard 3GPP in [51], we employ the urban model (UMA), which accounts for the channel frequency and the distance between the BS and the user. Additionally, for the penetration loss of the buildings, we consider both low and high building loss values obtained from the ECC report 302 and ITU-R P.2109 recommendation [52,53]. In this work, we leave the dynamic path loss model as future work, as it has not been standardized yet.

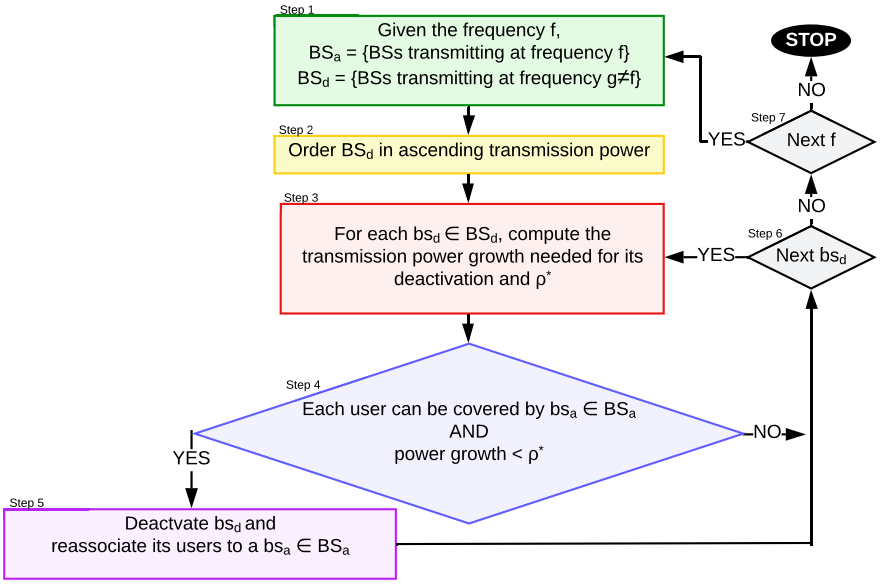

Fig. 4. Different steps of the Energy Reduction Strategy.

Once each user is associated with a BS, if possible, the transmitting power of each BS is decreased until it reaches the minimum required, i.e., until the path loss experienced by its users exceeds the allowable maximum.

4.4. Energy reduction strategy

Following the association procedure, the energy reduction strategy is implemented through the gradual switching of BSs. Its flow chart is drawn in Fig. 4. As depicted in the figure, the BSs are grouped into two sets: the *active* BSs denoted as BS_a (intended to remain active) and the *deactivating candidates* BSs denoted as BS_d (intended to switch to sleep mode). The BS_a set comprises BSs transmitting at frequency f, where $f \in$ 800 MHz, 2100 MHz, 3500 MHz, while the BS_d set includes BSs operating at a different frequency g with $f \neq g$. The BSs in BS_d are ordered in ascending order based on their transmission power (see step 2 in Fig. 4). This ordering is motivated by the observation that the least power-transmitting BSs are less efficient than the most power-transmitting ones, resulting in a larger energy requirement to carry a unit of traffic in the former [54].

For each BS bs_d in the BS_d set, we verify if the switching conditions are satisfied (steps 3 and 4 in Fig. 4). Specifically, we check if:

1. The users associated with bs_d can be reassigned to a BS within the BS_a set. This requires, for each user associated with bs_d, at least one BS bs_a in the BS_a set to:
   (a) Have enough available capacity to support the user.
   (b) Provide an experienced path loss lower than the allowable maximum.

   Conditions (b) may be met by increasing the transmitted power of bs_a, provided it remains below its maximum (see Table 1).
2. After verifying condition (1) for each user associated with bs_d, we check if the deactivation of bs_d is advantageous for reducing energy consumption in the network. As mentioned earlier, to cover bs_d's users, the transmission power of the active BSs may increase, up to the maximum possible (see Table 1). If this increase is lower than a given threshold ρ^*, then deactivating bs_d is beneficial for reducing the network's energy consumption. The value of the threshold is discussed in the next section and depends on the relationship between power requirement and transmitting power level of both the active BSs and the BS bs_d, intended to switch to sleep mode.

If conditions (1) and (2) are verified, bs_d is deactivated (step 5 in Fig. 4). Its users are then associated with an active BS from the BS_a set, following two possible approaches:

- *Transmission Power-Based (TX-B)*: Each user is associated with the active BS in BS_a, requiring the minimum growth of the transmission power to cover the given user.
- *Path Loss-Based (PL-B)*: In this approach, the current user is associated with the active BS in BS_a that minimizes the experienced path loss.

If conditions (1) or (2) are not met, the process moves to the next BS in the BS_d set, if possible (step 5 in Fig. 4). This procedure is repeated for each operating BS frequency, f, among the three at which the BSs operate: 800 MHz, 2100 MHz, 3500 MHz (step 7 in Fig. 4).

5. Key performance indicators

This section explains the KPIs considered in this study.

Transmitted (TX) power (dBm)

This represents the total transmitted power of the active BSs, in dBm.

Power requirement (W)

It is measured as the sum of the power consumed by each BS in the network, in watt. Some BSs are active and require power supply, while others are in sleep mode and do not need power supply. The power requirement of an active BS is computed as in (1). Similar to [31], the power needs of the BS in sleep mode are considered negligible. Indeed, it ranges between 0.1 W and 86 W, according to [41,55], which is much lower than 262 W, needed by an idle BS, as depicted in Fig. 1.

Active BSs

This represents the number of BSs that the energy reduction strategy keeps active.

6. Threshold ρ^*

As mentioned in Section 4, one of the conditions for the deactivation of a BS is leveraging a reduction in network energy consumption. This occurs when, for a given BS bs_d, the network's energy consumption is higher when it is active than when it is deactivated, despite the increased transmitting power of the active BSs required to cover its users.

Eq. (1) illustrates that the power consumption of a BS consists of a fixed cost and a contribution dependent on the BS transmitting power. Thus, the power need can be formulated as:

$$P_c^{(t)} = \bar{P} + K \cdot P^{(t)} \tag{2}$$

where

$$\bar{P} = N_A(P_T + P_{DSP}) + P_R + P_C + P_B \tag{3}$$

$$K = \frac{N_A}{\eta} \tag{4}$$

Here N_A is the number of antenna elements, P_T and P_{DSP} are the power needed by the radio frequency transceiver and the digital signal processing, in W. The parameter η is the efficiency of the power amplifier. P_R, P_C, and P_B are the power drained by the rectifier, the cooling system, and the backhaul link, respectively, in W. (see Table 2). $P^{(t)}$ is the transmitted power in watt. As reported in Table 3, for 800 MHz and 2100 MHz BSs, $\bar{P}$ is 265.5 W, while for 3500 MHz BSs, it is 420 W. The value of K is 2 for 800 MHz BSs and 2100 MHz BSs, and 128 for 3500 MHz BSs.

Deactivating a BS bs_d reduces the network power requirement if the following inequality is satisfied:

$$\sum_{a \in BS_a} (K_a P_a^{(t)} + \bar{P}_a) + K_d P_d^{(t)} + + \bar{P}_d > \sum_{a \in BS_a} (K_a \tilde{P}_a^{(t)} + \bar{P}_a) \tag{5}$$

where K_a, K_d, $\bar{P}_a$ and $\bar{P}_d$ are, respectively, the K parameter of (4) and the $\bar{P}$ parameter of (3), for the active BSs and those we intend to deactivate. $P_a^{(t)}$ represents the transmission power for the active BSs, while $P_d^{(t)}$ corresponds to the transmission power for the BS intended for deactivation, bs_d. $\tilde{P}_a^{(t)}$ is the transmission power of the active BS, after the deactivation of BS bs_d. From this inequality, we derive the upper bound for the maximum growth of the transmitting power of the BSs that remain active:

$$\sum_{a \in BS_a} (\tilde{P}_a^{(t)} - P_a^{(t)}) < \frac{\bar{P}_d}{K_a} + \frac{K_d}{K_a} P_d^{(t)} = \rho^* \tag{6}$$

This inequality reveals that when the growth of the transmitting power of the active BSs exceeds the computed upper bound, the additional cost to carry the traffic of the deactivated BS through the active ones does not compensate for the savings achieved by BS deactivation. Thus, the deactivation of a BS is beneficial for reducing network power requirement when the growth of the transmitted power from the BSs that remain active is bounded by ρ^*. This bound depends on the transmitting power of the BS that we want to deactivate and on the power requirement characteristics of both the considered BS and the BSs that remain active.

6.1. Numerical evaluation

In this section, we delve into the numerical values associated with the threshold ρ^*. To accomplish this, we employ a simplified scenario comprising two BSs differing in technologies and/or frequencies: one identified as the target for deactivation (bs_d) and the other as the one that remains active (bs_a). This implies that in this simplified scenario, only two of the three BS types considered in our work are involved. As mentioned in the previous section, to gain an advantage in terms of energy consumption, the active BSs can increase their transmission power to the value ρ^* computed in (6), provided that it remains below the maximum allowable transmission power, see Table 1.

Table 3
Values of the parameters for ρ^* computation.

Parameter	800 MHz	2100 MHz	5G 3500
K	2.0	2.0	2.0
$\bar{P}$ (W)	262.5	262.5	420.0

When there is a single BS that remains active, bs_a, the threshold in (6) is given by the minimum between the value computed in (6) and P_{MAX} - P_a, where P_{MAX} is the maximum transmission power of bs_a and P_a is its current transmission power. Figs. 5(a), 5(b), 5(c), 5(d), 5(e), and 5(f) present the values of ρ^* for the scenarios where the active and switching candidate technologies are, respectively, 800 MHz and 2100 MHz, 800 MHz and 3500 MHz, 2100 MHz and 800 MHz, 2100 MHz and 3500 MHz, 3500 MHz and 800 MHz, 3500 MHz and 2100 MHz. Please note that 800 MHz refers to a 5G NR BS with an omnidirectional antenna transmitting at 800 MHz, 2100 MHz refers to a 5G NR BS with an omnidirectional antenna transmitting at 2100 MHz, and 3500 MHz represents a 5G NR BS using beamforming, transmitting at 3500 MHz.

In each plot of Fig. 5, different curves represent varying levels of transmission power for the potentially deactivated BS (bs_d). The figures highlight that when the active technologies are 800 MHz and 2100 MHz (see Figs. 5(a), 5(b), 5(c), 5(d)), the upper bound is effectively determined by their maximum transmission power. This is evident as (6) consistently exceeds it for each transmission power of bs_d, providing values up to 326 and 163 times larger than the maximum transmission power in case the active BS operates at 800 MHz and 2100 MHz, respectively. Specifically, when bs_a operates on 800 MHz and 2100 MHz technology, ρ^* decreases from 39.81 W to 0 W and from 79.43 W to 0 W, respectively, as the transmission power of the active BS varies between 0 W and 39.81 W and between 0 W and 79.43 W. This holds true regardless of the transmitting power of the potentially deactivated BS, bs_d.

The scenario changes when 3500 MHz is the active technology. The transmission power of the potentially deactivated BS, bs_d, impacts the value of ρ^*. At higher values of transmission power of bs_d, ρ^* remains below 2.1 W, while with increased transmission power of bs_d, it grows by up to 60%, reaching values exceeding 3.29 W.

6.2. Threshold in meters

In this section, we assess the maximum growth of the transmission power of bs_a in terms of the expansion of its coverage radius, assuming both bs_a and bs_d are installed on a roof, 18.6 m above the ground. To do this, we utilize the propagation model for the Urban Scenario of the 3GPP TR 38.901 specification described in [51], considering both LoS and N-LoS cases.

The maximum allowable path loss, denoted as $\mathrm{PL}_{MAX}(\mathrm{p})$, where p is the BS transmission power in dBm, serves as the upper bound to ensure an acceptable quality of service and depends on the BS transmission power. The experienced path loss is contingent upon the distance d between the considered BS and the user, denoted as PL(d) [51]. We evaluate the maximum increase in the radius coverage of the active BS as the inverse function of the path loss $PL^{-1}(\mathrm{PL}_{MAX}(\mathrm{p}+\rho^*))$.

The maximum growth of the BS range corresponding to scenarios where the active and switching candidate technologies are 800 MHz and 2100 MHz, 800 MHz and 3500 MHz, 2100 MHz and 800 MHz, 2100 MHz and 3500 MHz, 3500 MHz and 800 MHz, 3500 MHz and 2100 MHz is presented in Figs. 6(a), 6(b), 6(c), 6(d), 6(e), and 6(f), for the LoS and NLoS cases, marked by circles and triangles, respectively. The different curves in these plots represent various levels of transmission power for the potentially deactivated BS (bs_d). In previous section, we observe that if bs_a operates at 800 MHz or 2100 MHz, there is no impact on p_d, as ρ^* is constrained by the maximum transmission power, as discussed in the previous section. When bs_a is 800 MHz (Figs. 6(a),

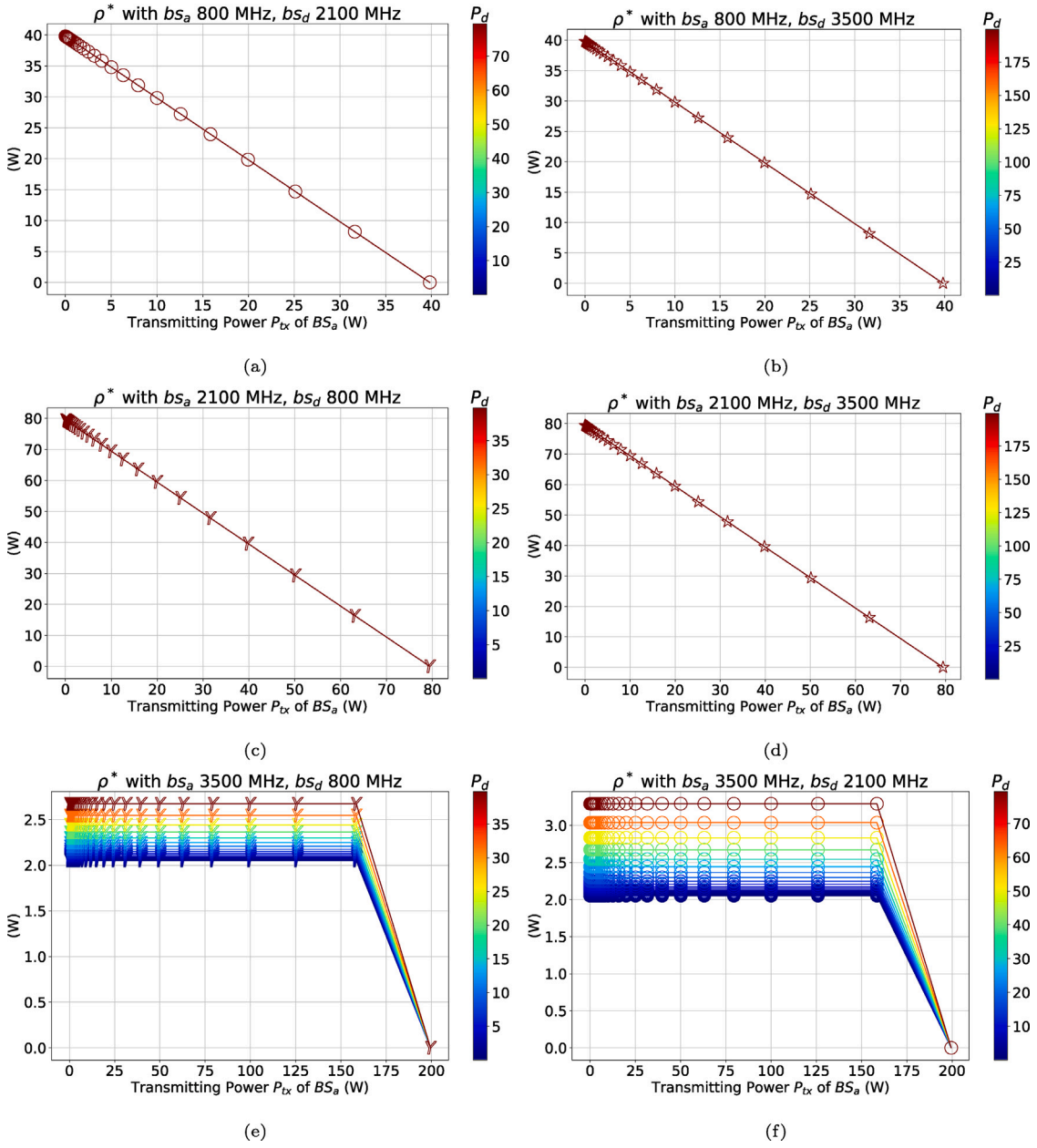

Fig. 5. Values of the threshold ρ^* for when the active and the switching candidate BS are, respectively (a) 800 MHz and 2100 MHz, (b) 800 MHz and 3500 MHz, (c) 2100 MHz and 800 MHz, (d) 2100 MHz and 3500 MHz, (e) 3500 MHz and 800 MHz, (f) 3500 MHz and 2100 MHz.

6(b)), the radius grows up to 3.3 km and 736 m, for users in LoS and NLoS, respectively. Slightly larger values, up to 3.8 km for LoS and 523 m for NLoS, are reached if bs_a operates at 2100 MHz, because of the larger power levels that can transmit than 800 MHz BSs, see Figs. 6(c), 6(d). Despite with 3500 MHz BSs the values of ρ^* are significantly lower than for 800 MHz or 2100 MHz BSs, see Fig. 5, its BS radius can rise up to 2.6 km and 302 m, for LoS and NLos, respectively, sightly lower than what reached with 2100 MHz and larger than in case of 800 MHz. This is due to the improvements in signal propagation introduced by the MA MIMO technology.

7. Performance evaluation

To assess the performance of the methodology presented in Section 4, we conducted 30 simulations, and we present the results as averages across them. We use the *Always On (A-ON)* scenario in which all the BSs always active as benchmark. We refer to the approach that uses transmission-based and path loss-based re-association, presented in Section 4, as *TX-B* and *PL-B*, respectively.

7.1. Comparison of the different energy reducing strategy

Before analyzing the power requirements of the different energy strategies, we first assess user coverage. User coverage is measured as the percentage of users that the RAN is able to serve, and it reaches 100% with each of the energy-reducing strategies. Figs. 7(a) and 7(b) present the power requirements and total transmission power, respectively. In Fig. 7(c), we show the number of BSs intended to switch to sleep mode but remain active because deactivating them would require

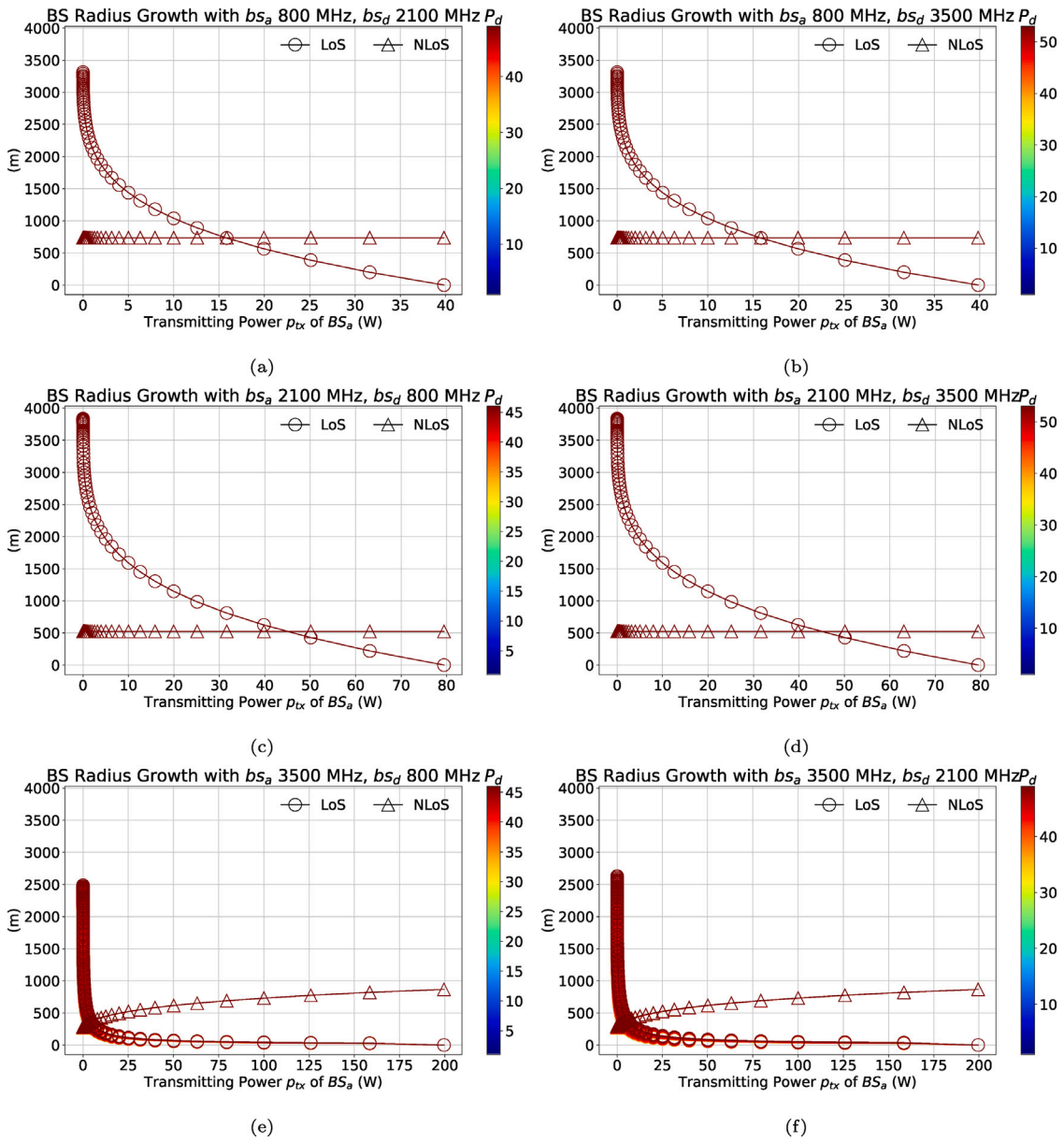

Fig. 6. The maximum growth of the BS range, in m, when the active and the switching candidate BS are, respectively (a) 800 MHz and 2100 MHz, (b) 800 MHz and 3500 MHz, (c) 2100 MHz and 800 MHz, (d) 2100 MHz and 3500 MHz, (e) 3500 MHz and 800 MHz, (f) 3500 MHz and 2100 MHz.

an increase in the transmission power of the active BSs beyond the threshold ρ^* (see Section 4). Additionally, Fig. 7(d) displays the number of BSs intended to switch to sleep mode but cannot, as deactivating them would leave some users uncovered. Finally, Fig. 7(e) reports the number of active BSs.

We report these results for *TX-B*, *PL-B*, and *A-ON* in blue, orange, and green, respectively. On the x-axis, we vary the order of the frequency intended to be active in each iteration of the energy-reducing strategy. From Fig. 7(a), we notice that our methodology significantly outperforms the benchmark *A-ON* scenario. Indeed, the reduction of the power requirement ranges between 11% and 76% when *PL-B* is used, while from 12% to 73% if *TX-B* is employed. *PL-B* approach usually provides a slightly lower power requirement than *TX-B*, despite it transmits more power than both *TX-B* and *A-ON*. Indeed, its network total transmission power accounts for up to 1533 dBm, 63% and 35% larger than in case of *TX-B* and *A-ON* employment, respectively, that use less than 997 dBm and 562 dBm for their transmission, see Fig. 7(b). Meanwhile, the number of active BSs with the *PL-B* and *TX-B* is almost identical ranging between 42 ad 132, up to 73% less than in the *A-ON* scenario, as shown in Fig. 7(e).

These results reveal that, as extensively demonstrated in literature for 4G ecosystems, also for 5G environments, having a few BSs that use high power levels for their transmission is more energy efficient than using many BSs that transmit at low power levels.

In addition, Fig. 7(c) reveals that *TX-B* incurs more often than *PL-B* in the impossibility to deactivate some BSs because the needed growth of the active BSs for covering the uncovered users is larger than the threshold ρ^*. Thus, while in the former case, this occurs no more than 66 times, in the latter up to 79. When associating users who have remained uncovered because of a BS deactivation, *TX-B* selects the active BS which needs the lowest growth of its transmission power. As a result, having low level of transmitting power is more likely than with *PL-B* (see Fig. 7(b)). This generates low values of ρ^* that make the satisfaction of the deactivation constraint difficult. On the contrary, the impossibility to deactivate some BSs because some users would remain uncovered occurs almost the same number of times, using the different approaches (see Fig. 7(d)).

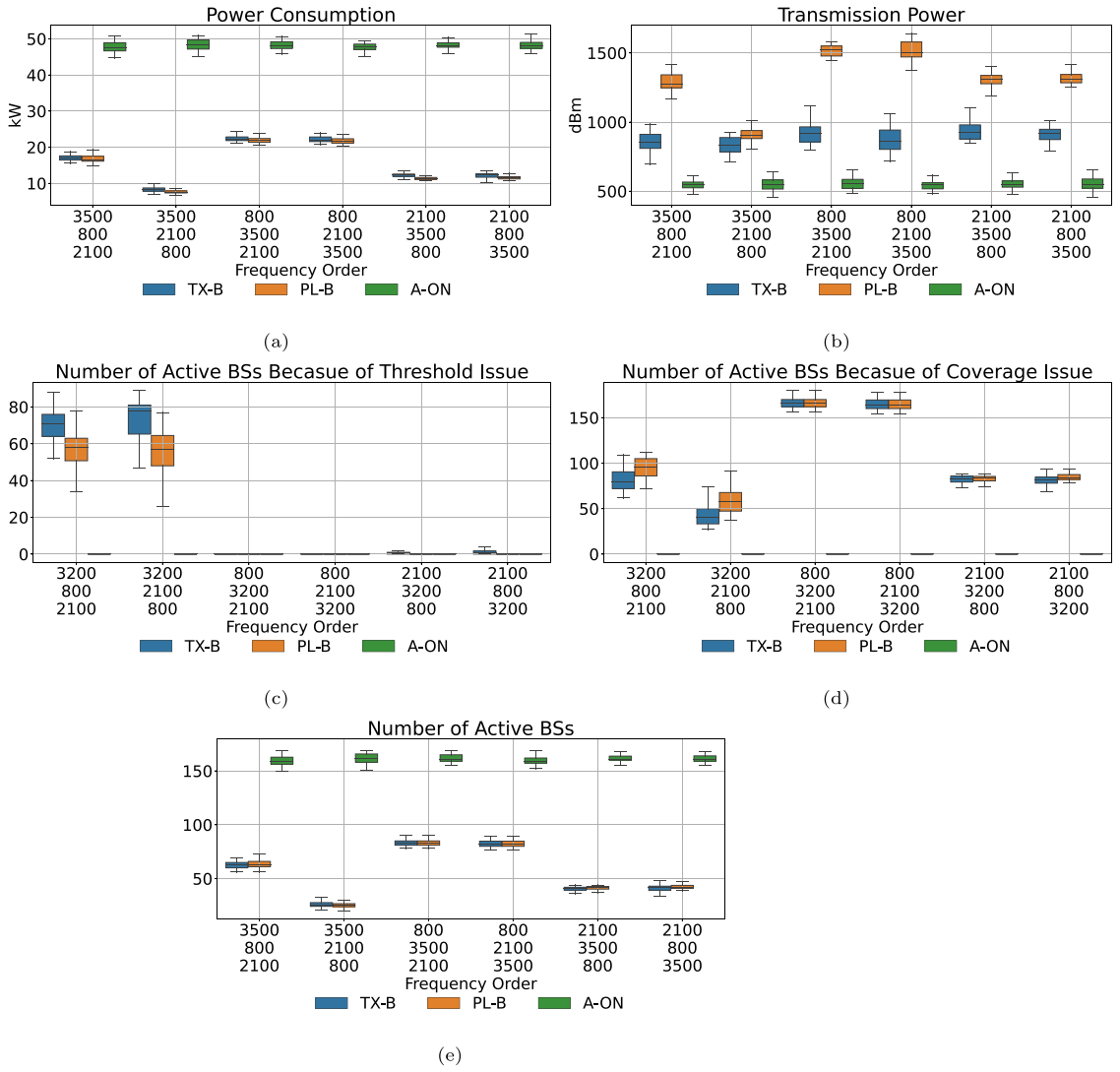

Fig. 7. Power requirement (a), in kW, transmitted power (b), in dBm, the instances of missed deactivation due to threshold exceeding (c), those due to the impossibility of covering the users (d), and the number of active BSs (e), with *TX-B* and *PL-B* and *A-ON* and varying the frequency order of the energy reducing strategy.

Finally, Fig. 7 demonstrates the impact of the frequency order in the energy-reducing strategy on performance. Specifically, with *PL-B* and *TX-B*, maintaining the active status of 3500 MHz, 800 MHz, and 2100 MHz BSs results in a power requirement of no more than 17 kW, which is 70% higher than the scenario where 3500 MHz, 2100 MHz, and 800 MHz is the frequency order, keeping the consumption below 10.4 kW. Similarly, initiating the activation of 800 MHz BSs leads to a network energy consumption ranging between 21 kW and 22 kW, while beginning with the activation of 2100 MHz BSs results in a lower consumption of 11 kW. For a more in-depth understanding of these findings, we will analyze the results at each frequency step in the next section.

7.2. Impact of the frequency order

In this section, we analyze the KPIs at each iteration of the energy reduction strategy, i.e., at step 7 in Fig. 4, when each BS in BS_d has been deactivated, if possible. Figs. 8(a), 8(b), 8(c), 8(d) and 8(e) illustrate power requirement, the number of deactivated BSs, instances of missed deactivation due to threshold exceeding, those due to the impossibility of covering the users and the number of active BSs, respectively, when *PL-B* is employed. These figures present the results with variations on the x-axis representing the order of the values of the frequency f of the BSs intended to remain active. The blue bars in the figures represent values before initiating the energy reduction strategy (at the end of step 3 in Fig. 3), while the orange, green, and red bars indicate results after the first, second, and third iterations, respectively. In Fig. 8(e), the different color gradient distinguishes the different technology of the BSs, as indicated by the grayscale in the legend. Clearly, as shown in Fig. 8, at *Iteration 0*, the results are identical for each possible frequency order. The figure highlights that when the first iteration keeps the BSs that use 800 MHz or 2100 MHz active, that iteration deactivates up to 120 BSs, but the following ones do not deactivate any other BSs (Fig. 8(b)), rendering them ineffective in further improving energy savings (see Fig. 8(a)). This is because, in these cases, from the second iteration (green bars in the figures), the deactivation of BSs is not possible due to coverage problems. As shown in Fig. 8(e), the first iteration deactivates each BS of the technologies that are intended to be deactivated, making users uncovered in case of further deactivation at the following iterations (see Fig, 8(d)). Fig. 8(a) indicates that keeping 2100 MHz BSs active at the first iteration consumes no more than 12 kW, lower than 22 kW obtained when 800 MHz

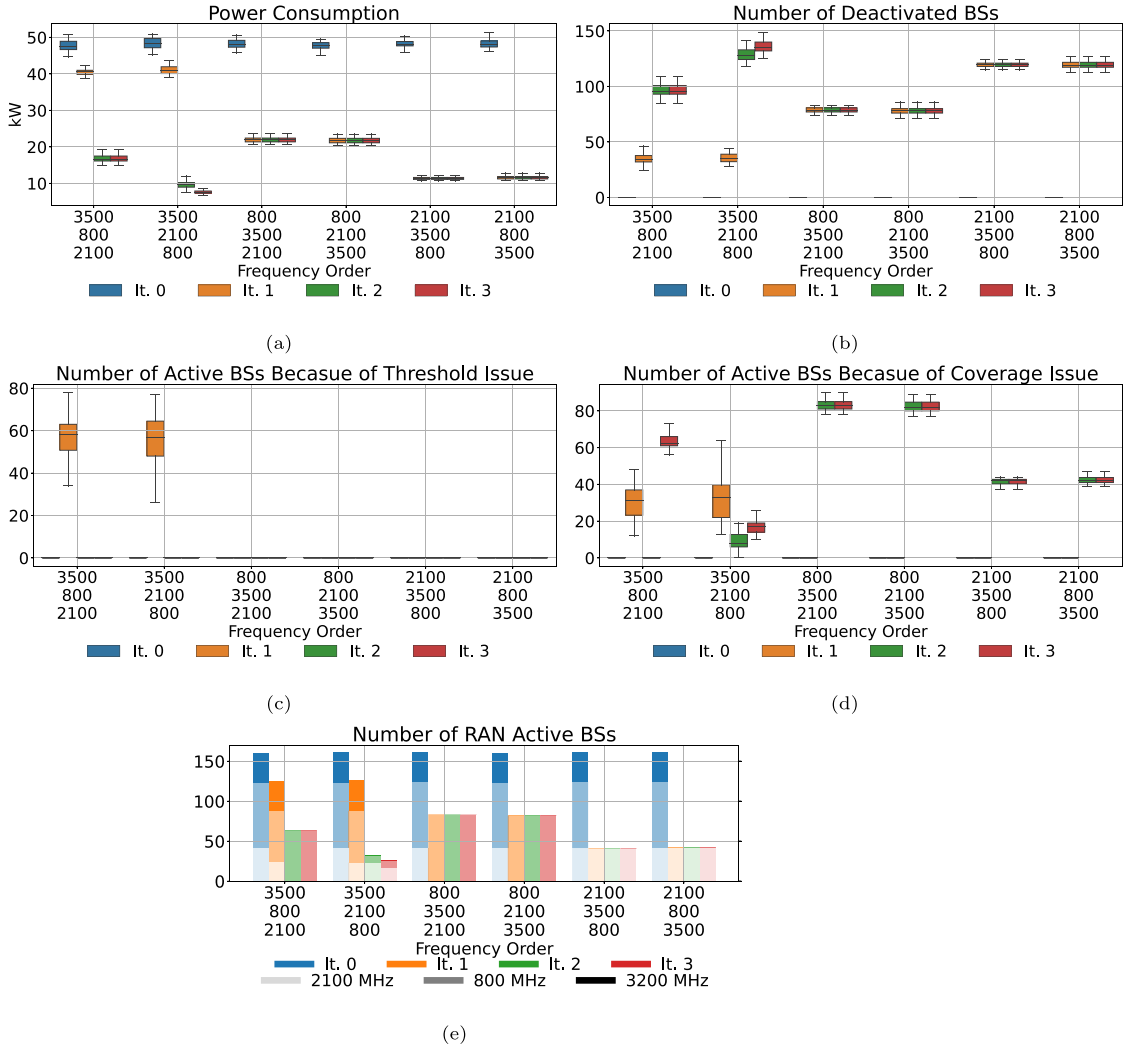

Fig. 8. Power requirement (a), in kW, the number of deactivated BSs (b), the instances of missed deactivation due to threshold exceeding (c), those due to the impossibility of covering the users (d) and the number of active BSs (e), with *TX-B* and *PL-B* and *A-ON* at each iteration of the power reduction power.

BSs remain active at the first iteration. Indeed, in the former case, up to 120 BSs are deactivated, 53% more than in the latter (Fig. 8(b)). Despite the low frequency, 800 MHz BSs have a shorter coverage range than 2100 MHz ones (see Fig. 6), due to its strict constraint on the maximum transmitting power, as shown in Table 1.

The scenario varies when the 3500 MHz BSs are kept active at the first iteration. If this is the case, no more than 36 BSs are deactivated during the initial iteration (see Fig. 8(b)), leaving active 64 800 MHz BSs and 24 2100 MHz BSs (see Fig. 8(e)). This is attributed to the low values that ρ^* takes on when the active frequency is 3500 MHz and the inability to cover users who remain uncovered due to BS deactivation. The former makes the deactivation of up to 58 BSs inconvenient (Fig. 8(c)). The latter prevents the deactivation of up to 32 BSs since the BSs that operate at 3500 MHz can support only a few users (Fig. 8(d)). As depicted in Fig. 8(a), the frequency order that yields the best performance is 3500 MHz, 2100 MHz, and 800 MHz, consuming no more than 7.6 Kw, up to 65% lower than the other cases. Initiating the process by keeping the 3500 MHz BSs active does not deactivate many BSs (no more than 36). However, when we subsequently keep the 2100 MHz BSs active, whose radio coverage is the longest among the different BS types, it helps alleviate the user coverage problem during deactivation of the following iterations. User coverage issues are also mitigated because, in the previous iteration, we did not deactivate many BSs.

7.3. The impact of the threshold

In this section, we compare the performance of our proposed methodology with approaches from the literature. Specifically, similar to the approaches in [56–58], we consider a methodology that deactivates BSs in order of their transmitted power, from the BS transmitting the least to the one transmitting the most, without any constraint on the maximum allowed increase in transmitted power (*NO-TH*). In practice, this method uses the energy reduction strategy described in Section 4, where ρ^* is set to infinity. This means that a BS is deactivated if all its users can be covered by other active BSs, regardless of the required increase in transmission power. Next, we apply two strategies based on the geographical distribution density of the BSs. As in [59], the BSs located with coverage redundancy are deactivated. For doing this, the strategy calculates the average distance of each BS to its 5 nearest BSs and orders them from the smallest to the largest average distance. Then, following this order, each BS is deactivated with a certain probability, provided its users can be covered by other active BSs. The probability is set to one for the distance-based approach (*D-B*), or inversely proportional to the average distance from other BSs in the distance-proportional approach (*DP-B*). Figs. 9(a) and 9(b) depict the power needs, in kW, with frequency orders of 3500 MHz, 2100 MHz, 800 MHz, and 2100 MHz, 3500 MHz, 800 MHz, respectively, which require the lowest amount of power. The blue, orange, green,

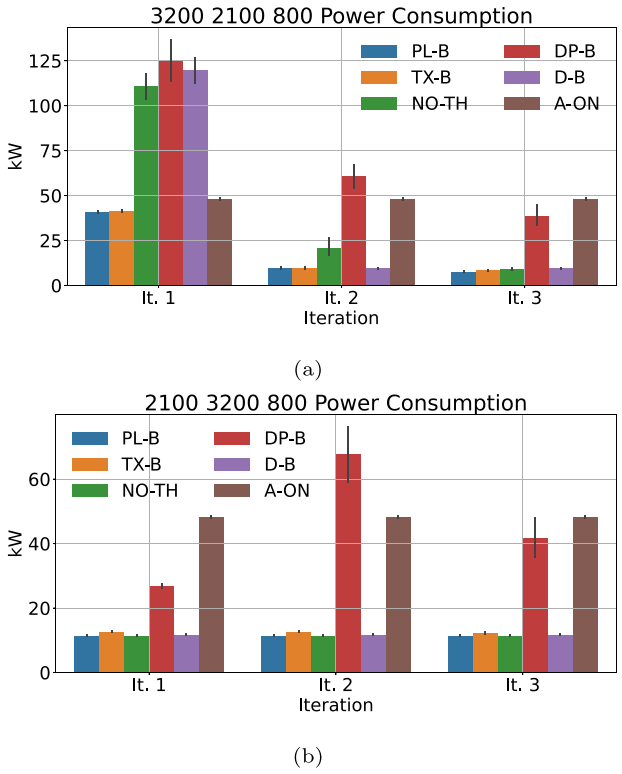

Fig. 9. Power requirement, in kW, with 3500 MHz, 2100 MHz, 800 MHz (a) and 2100 MHz, 3500 MHz, 800 MHz (b) as frequency order, at each iteration of the energy reduction strategy.

red, purple and brown bars represent the energy consumption for scenarios *PL-B*, *TX-B*, *NO-TH*, *DP-B*, *D-B* and *A-ON* (BSs always active), respectively. Each set of bars in the plots corresponds to the energy consumption at the conclusion of different iterations of the energy reduction strategy.

From the figures, it is evident that when the frequency order is 3500 MHz, 2100 MHz, 800 MHz (see Fig. 9(a)), after the first and second iterations, the *TX-B* and *PL-B* approaches need up to 63% less power than the other scenarios. Ultimately, at the third iteration, *TX-B* and *PL-B* require 16% and 84% less power than *NO-TH* and *A-ON*, respectively.

Notably, at the end of the first iteration, *NO-TH*, *DP-B* and *D-B* require the largest amount of power, exceeding 120 kW, even surpassing *A-ON* by up to 62%. This discrepancy arises because *NO-TH*, *DP-B* and *D-B* deactivate both 2100 MHz and 800 MHz BSs, despite the increased transmission power of 3500 MHz BSs required to cover the users of disconnected BSs. At the end of the second iteration, these three approaches significantly reduce their power requirement. *D-B* uses 10 kW, comparable to values obtained with *TX-B* and *PL-B*. Conversely, *NO-TH* and *DP-B* require, respectively, 21 kW and 61 kW, remaining 54% and 85% larger than *TX-B* and *PL-B*. At the end of the third iteration, *NO-TH* and *D-B* need no more than 9 kW, while *DP-B* up to 39 kW, resulting in 81% and 19%, respectively less than *A-ON*, and 11% and 79% more than *TX-B* and *PL-B*.

When the frequency order is 2100 MHz, 3500 MHz, and 800 MHz, the reduction in power requirements can reach up to 76% when BSs are deactivated, compared to the *A-ON* scenario, as discussed in previous sections. Fig. 9(b) highlights that *NO-TH* and *D-B* provide almost the same performance as *TX-B* and *PL-B*. This is due to the values that the threshold ρ^* assumes. As discussed in Sections 6 and 7, when 2100 MHz BSs are intended to remain active, then ρ^*, as computed in Eq. (6), exceeds the maximum transmission power. This means that the growth in transmission power is actually limited by this maximum value. As a result, deactivating a BS is always advantageous for reducing power requirements, regardless of how much the transmission power must increase to cover its users. For the *DP-B* strategy, more power is needed for the network supply than the other approaches because, unlike in *D-B*, a BS is switched to sleep mode with a probability less than 1, and this probability decreases as the average distance from other BSs increases.

8. Lesson learnt

In this section, we discuss the main aspects that have emerged in our work. We introduce a BS switching strategy designed for multi-frequency and multi-technology BSs in the RAN. This proposed approach gradually deactivates different types of BSs, making switching decisions based on a threshold parameter. This parameter depends on the transmission power of the BS intended for deactivation and on the power requirement characteristics of the BS. The threshold determines the maximum permissible increase in transmission power for active BSs, ensuring coverage for users affected by BS deactivation while achieving a reduction in power needs.

First, our formulation of the threshold guiding the BS deactivation decision highlights that, with 3500 MHz BSs, its values are lower than 2.6 W, notably lower compared to those for 800 MHz or 2100 MHz BSs. Despite this, the BS radius of these BSs can extend up to 2.5 km (LoS), slightly lower than that achieved with 2100 MHz and 800 MHz BSs. This is attributed to the enhancements in signal propagation introduced by the MA MIMO technology.

Second, our evaluations illustrate that, akin to the well-documented observations in 4G environments, the energy efficiency of 5G ecosystems is higher when a limited number of BSs operate at higher power levels compared to employing numerous BSs transmitting at lower power levels. Moreover, the order of the BS types guiding the BS deactivation impacts the achieved performance. Initiating the process by retaining active 3500 MHz BSs results in the deactivation of a limited number of BSs. Nevertheless, when subsequently maintaining the activity of 2100 MHz BSs, which have the longest radio coverage among the various BS types due to a higher maximum allowed transmission power level, it effectively addresses the user coverage challenge during subsequent deactivation iterations. For the same reason, when 2100 MHz BSs are kept active in the first iteration, the power requirements are lower compared to when the 800 MHz BSs are intended to remain active initially. This is because, in the former case, the radio coverage is longer than in the latter, thanks to its stringent constraint on the maximum transmitting power, aiding in mitigating the user coverage issue during the deactivation of subsequent iterations. Understanding the achievement in power requirement drop at each iteration is fundamental to gaining insight into the intermediate steps that are achievable if the operator prefers gradually deactivating BS technologies (for example, one technology per hour). If this is the case, using the threshold is strictly necessary when 3500 MHz is intended to remain active. Indeed, in such cases, the low transmission power of the BSs that are supposed to be deactivated significantly constrains the transmission power growth of the active BSs needed to cover the users who remain disconnected.

Finally, re-associating users who remain uncovered after a BS deactivation based on the criterion of minimizing transmission power tends to result in a lower level of transmitting power compared to re-associations using path loss-based minimization policies. This results in lower values of the threshold and makes it challenging to meet the deactivation constraint.

9. Conclusion

In this work, we propose a comprehensive BS switching strategy based on a threshold, designed for realistic multi-frequency and multi-technology BSs within the RAN. Our strategy deactivates BSs if the

growth of the transmission power needed to cover the users who remained uncovered due to deactivation is bounded by a threshold. This threshold is determined using the power requirements characteristics of both the deactivated BS and the BSs that remain active. We evaluate our proposed methodology through simulation of a realistic RAN located in a urban environment and the results are promising, achieving up to 73% energy savings without any degradation in Quality of Service. We quantify the influence of the frequency order of BS deactivation and examine user re-association strategies aimed at minimizing either path loss or transmission power.

As part of future work, we plan to incorporate a dynamic path loss model and account for user mobility. This includes considering the frequency of the process that determines whether to put a BS into sleep mode, ensuring the network remains aligned with user dynamics.

CRediT authorship contribution statement

Greta Vallero: Writing – original draft, Software, Methodology, Formal analysis, Data curation, Conceptualization. **Michela Meo:** Writing – review & editing, Supervision, Project administration, Funding acquisition. **Wout Joseph:** Writing – review & editing, Supervision. **Margot Deruyck:** Writing – review & editing, Supervision, Conceptualization.

Declaration of competing interest

The authors declare that they have no known competing financial interests or personal relationships that could have appeared to influence the work reported in this paper.

Acknowledgments

This paper was supported by the European Union under the Italian National Recovery and Resilience Plan (NRRP) of NextGenerationEU, partnership on "Telecommunications of the Future" (PE00000001 - program "RESTART", Focused Project R4R).

This article is based upon work from COST Action INTERACT, CA20120, supported by COST (European Cooperation in Science and Technology).

Data availability

The data that has been used is confidential.

References

[1] AT&T, Progress to 2025 — 10x goal update, 2019, https://about.att.com/ecms/dam/csr/2019/reducing-emissions/10x-ProgressReport-2018.pdf (Accessed 17 January 2025).

[2] Vodafone Group, Sustainable business report 2019, 2019, https://www.gsma.com/betterfuture/wp-content/uploads/2019/10/2019-09-24-a60d6541465e86561f37f0f77ebee0f7-1.pdf (Accessed 17 January 2025).

[3] Vodafone Business, Vodafone internet of things (IoT) - smart grid and metering, 2022, URL https://www.vodafone.com/business/iot/end-to-end-solutions/smart-grid-and-metering (Accessed 17 January 2025).

[4] Keysight Technologies, Next generation wireless: A guide to the fundamentals of 6G, 2023, URL https://www.keysight.com/at/de/assets/7123-1050/ebooks/Next-Generation-Wireless-A-Guide-to-the-Fundamentals-of-6G.pdf (Accessed 17 January 2025).

[5] Intergovernmental Panel on Climate Change (IPCC), Global warming of 1.5 °c, Spec. Rep. (2018) URL https://www.ipcc.ch/site/assets/uploads/sites/2/2022/06/SR15_Full_Report_HR.pdf (Accessed 17 January 2025).

[6] L.M. Larsen, H.L. Christiansen, S. Ruepp, M.S. Berger, Toward greener 5G and beyond radio access networks—A survey, IEEE Open J. Commun. Soc. 4 (2023) 768–797.

[7] P. Kaur, R. Garg, V. Kukreja, Energy-efficiency schemes for base stations in 5G heterogeneous networks: a systematic literature review, Telecommun. Syst. 84 (1) (2023) 115–151.

[8] W. Tan, S. Li, M. Zhou, Spectral and energy efficiency for uplink massive MIMO systems with mixed-ADC architecture, Phys. Commun. 50 (2022) 101516.

[9] A. Salh, L. Audah, Q. Abdullah, Ö. Aydoğdu, M.A. Alhartomi, S.H. Alsamhi, F.A. Almalki, N.S.M. Shah, Low computational complexity for optimizing energy efficiency in mm-wave hybrid precoding system for 5G, IEEE Access 10 (2021) 4714–4727.

[10] G. Castellanos, S. De Gheselle, L. Martens, N. Kuster, W. Joseph, M. Deruyck, S. Kuehn, Multi-objective optimisation of human exposure for various 5G network topologies in Switzerland, Comput. Netw. 216 (2022) 109255.

[11] S. Alotaibi, Key challenges of mobility management and handover process in 5G HetNets, Int. J. Comput. Sci. Netw. Secur. 22 (4) (2022) 139–146.

[12] Y. Ramamoorthi, A. Kumar, Resource allocation for CoMP in cellular networks with base station sleeping, IEEE Access 6 (2017) 12620–12633.

[13] H. Chen, Y. Li, J.L. Rebelatto, B.F. Uchoa-Filho, B. Vucetic, Harvest-then-cooperate: Wireless-powered cooperative communications, IEEE Trans. Signal Process. 63 (7) (2015) 1700–1711.

[14] Ericsson, Ericsson mobility report november 2022, 2022, URL https://www.ericsson.com/4ae28d/assets/local/reports-papers/mobilityreport/documents/2022/ericsson-mobility-report-november-2022.pdf.

[15] J.S. Pujol-Roigl, S. Wu, Y. Wang, M. Choi, I. Park, Deep reinforcement learning for cell on/off energy saving on wireless networks, in: 2021 IEEE Global Communications Conference, GLOBECOM, IEEE, 2021, pp. 01–07.

[16] K. Tan, D. Bremner, J. Le Kernec, Y. Sambo, L. Zhang, M.A. Imran, Graph neural network-based cell switching for energy optimization in ultra-dense heterogeneous networks, Sci. Rep. 12 (1) (2022) 21581.

[17] S. Han, S. Bian, et al., Energy-efficient 5G for a greener future, Nat. Electron. 3 (4) (2020) 182–184.

[18] O. Blume, D. Zeller, U. Barth, Approaches to energy efficient wireless access networks, in: 2010 4th International Symposium on Communications, Control and Signal Processing, ISCCSP, IEEE, 2010, pp. 1–5.

[19] N. Piovesan, D. López-Pérez, M. Miozzo, P. Dini, Joint load control and energy sharing for renewable powered small base stations: A machine learning approach, IEEE Trans. Green Commun. Netw. 5 (1) (2020) 512–525.

[20] Y. Wang, X. Dai, J.M. Wang, B. Bensaou, A reinforcement learning approach to energy efficiency and QoS in 5G wireless networks, IEEE J. Sel. Areas Commun. 37 (6) (2019) 1413–1423.

[21] N.B. Rached, H. Ghazzai, A. Kadri, M.-S. Alouini, A time-varied probabilistic ON/OFF switching algorithm for cellular networks, IEEE Commun. Lett. 22 (3) (2018) 634–637.

[22] T.E. Mathonsi, T.M. Tshilongamulenzhe, Intelligent energy efficiency algorithm for the 5G dense heterogeneous cellular networks, in: 2020 International Conference on Computational Science and Computational Intelligence, CSCI, 2020, pp. 144–149, http://dx.doi.org/10.1109/CSCI51800.2020.00032.

[23] M.S. Hossain, A. Jahid, K.Z. Islam, M.H. Alsharif, K.M. Rahman, M.F. Rahman, M.F. Hossain, Towards energy efficient load balancing for sustainable green wireless networks under optimal power supply, IEEE Access 8 (2020) 200635–200654.

[24] D. Renga, H.A.H. Hassan, M. Meo, L. Nuaymi, Energy management and base station on/off switching in green mobile networks for offering ancillary services, IEEE Trans. Green Commun. Netw. 2 (3) (2018) 868–880.

[25] M. Ali, M. Meo, D. Renga, Cost saving and ancillary service provisioning in green mobile networks, in: The Internet of Things for Smart Urban Ecosystems, Springer, 2019, pp. 201–224.

[26] N.G. Veerappan Kousik, Y. Natarajan, K. Suresh, R. Patan, A.H. Gandomi, Improving power and resource management in heterogeneous downlink OFDMA networks, Information 11 (4) (2020) 203.

[27] S. Ashtari, F. Tofigh, M. Abolhasan, J. Lipman, W. Ni, Efficient cellular base stations sleep mode control using image matching, in: 2019 IEEE 89th Vehicular Technology Conference, VTC2019-Spring, IEEE, 2019, pp. 1–7.

[28] M. Deruyck, W. Joseph, E. Tanghe, L. Martens, Reducing the power consumption in LTE-advanced wireless access networks by a capacity based deployment tool, Radio Sci. 49 (9) (2014) 777–787.

[29] M. Deruyck, D. Renga, M. Meo, L. Martens, W. Joseph, Reducing the impact of solar energy shortages on the wireless access network powered by a PV panel system and the power grid, in: 2016 IEEE 27th Annual International Symposium on Personal, Indoor, and Mobile Radio Communications, PIMRC, IEEE, 2016, pp. 1–6.

[30] M. Deruyck, D. Renga, M. Meo, L. Martens, W. Joseph, Accounting for the varying supply of solar energy when designing wireless access networks, IEEE Trans. Green Commun. Netw. 2 (1) (2018) 275–290.

[31] G. Vallero, D. Renga, M. Meo, M.A. Marsan, Greener RAN operation through machine learning, IEEE Trans. Netw. Serv. Manag. 16 (3) (2019) 896–908.

[32] G. Vallero, M. Deruyck, M. Meo, W. Joseph, Base station switching and edge caching optimisation in high energy-efficiency wireless access network, Comput. Netw. 192 (2021) 108100, http://dx.doi.org/10.1016/j.comnet.2021.108100, URL https://www.sciencedirect.com/science/article/pii/S138912862100181X.

[33] G. Vallero, M. Deruyck, W. Joseph, M. Meo, Caching at the edge in high energy-efficient wireless access networks, in: ICC 2020 - 2020 IEEE International Conference on Communications, ICC, 2020, pp. 1–7, http://dx.doi.org/10.1109/ICC40277.2020.9149194.

[34] M. Matalatala, M. Deruyck, S. Shikhantsov, E. Tanghe, D. Plets, S. Goudos, K.E. Psannis, L. Martens, W. Joseph, Multi-objective optimization of massive MIMO 5G wireless networks towards power consumption, uplink and downlink exposure, Appl. Sci. 9 (22) (2019) 4974.
[35] 3rd Generation Partnership Project; Technical Specification Group Radio Access Network; NR; Physical channels and modulation (Release 17), 3rd Generation Partnership Project (3GPP), 2023, URL https://www.3gpp.org/ftp/Specs/archive/38_series/38.211/.
[36] 3rd Generation Partnership Project; Technical Specification Group Radio Access Network; NR; Base Station (BS) radio transmission and reception (Release 17), Technical Report TS 38.104, 3rd Generation Partnership Project (3GPP), 2023, URL https://www.3gpp.org/ftp/Specs/archive/38_series/38.104/.
[37] B. Thors, A. Furuskär, D. Colombi, C. Törnevik, Time-averaged realistic maximum power levels for the assessment of radio frequency exposure for 5G radio base stations using massive MIMO, IEEE Access 5 (2017) 19711–19719, http://dx.doi.org/10.1109/ACCESS.2017.2753459.
[38] R.. Schwarz, Be ahead in 5G - be ready for the future, 2021, https://www.rohde-schwarz.com/.
[39] ETSI, ETSI TS 136 213 v14.6.0 - LTE; Evolved Universal Terrestrial Radio Access (E-UTRA); Physical Layer Procedures (3GPP TS 36.213 version 14.6.0 Release 14), Technical report, ETSI, 2018.
[40] A. Fehske, G. Fettweis, J. Malmodin, G. Biczok, The global footprint of mobile communications: The ecological and economic perspective, IEEE Commun. Mag. 49 (8) (2011) 55–62.
[41] G. Auer, O. Blume, V. Giannini, I. Godor, M. Imran, Y. Jading, E. Katranaras, M. Olsson, D. Sabella, P. Skillermark, et al., D2. 3: Energy efficiency analysis of the reference systems, areas of improvements and target breakdown, Earth 20 (10) (2010).
[42] A. Israr, Q. Yang, A. Israr, Power consumption analysis of access network in 5G mobile communication infrastructures — An analytical quantification model, Pervasive Mob. Comput. 80 (2022) 101544, http://dx.doi.org/10.1016/j.pmcj.2022.101544, URL https://www.sciencedirect.com/science/article/pii/S1574119222000049.
[43] M. Deruyck, E. Tanghe, W. Joseph, W. Vereecken, M. Pickavet, L. Martens, B. Dhoedt, Model for power consumption of wireless access networks, IET Sci. Meas. Technol. 5 (4) (2011) 155–161.
[44] MAMMOET, Massive MIMO for efficient transmission: Deliverables 1.1, systems scenarios and requirements specifications, 2014.
[45] M. Matalatala, M. Deruyck, E. Tanghe, L. Martens, W. Joseph, et al., Performance evaluation of 5G millimeter-wave cellular access networks using a capacity-based network deployment tool, Mob. Inf. Syst. 2017 (2017).
[46] M. Matalatala, et al., Simulations of beamforming performance and energy efficiency for 5G mm-wave cellular networks, in: 2018 IEEE Wireless Communications and Networking Conference, WCNC, IEEE, 2018, pp. 1–6.
[47] Federal Office of Topography - Swisstopo, Geoinformation and Geodata, Technical Report, Federal Office of Topography - Swisstopo, 2022.
[48] Wikipedia contributors, Zurich, 2024, URL https://en.wikipedia.org/wiki/Zurich (Accessed 19 September 2024).
[49] E.T. ETSI, T. ETSI, 136 213 v14. 6.0-LTE; Evolved Universal Terrestrial Radio Access (E-UTRA); Physical Layer Procedures (3GPP TS 36.213 version 14.6. 0 Release 14), Technical Report, ETSI, 2018.
[50] Federal Communications Commission (ComCom), Mobile market share in Switzerland, 2021, 2021, (Accessed March 2021).
[51] E.T. ETSI, T. ETSI, 138 901 v15. 0.0-5G; Study On Channel Model for Frequencies from 0.5 to 100 GHz (3GPP TR 38.901 version 15.0. 0 Release 15), Technical Report, ETSI, 2018.
[52] Electronic Communications Committee (ECC), Sharing and Compatibility Studies Related to Wireless Access Systems Including Radio Local Area Networks (WAS/RLAN) in the Frequency Band 5925-6425 MHz, Technical Report 302, ECC, 2019.
[53] International Telecommunication Union (ITU), Recommendation ITU-R P.2109-1: Prediction of Building Entry Loss, (Technical Report P.2109-1) ITU, 2019, p. 7.
[54] G. Vallero, D. Renga, M. Meo, M.A. Marsan, RAN energy efficiency and failure rate through ANN traffic predictions processing, Comput. Commun. 183 (2022) 51–63.
[55] B. Debaillie, C. Desset, F. Louagie, A flexible and future-proof power model for cellular base stations, in: 2015 IEEE 81st Vehicular Technology Conference, VTC Spring, IEEE, 2015, pp. 1–7.
[56] L. Chiaraviglio, M. Listanti, E. Manzia, Life is short: The impact of power states on base station lifetime, Energies 8 (12) (2015) 14407–14426.
[57] L. Chiaraviglio, D. Ciullo, G. Koutitas, M. Meo, L. Tassiulas, Energy-efficient planning and management of cellular networks, in: 2012 9th Annual Conference on Wireless on-Demand Network Systems and Services, WONS, IEEE, 2012, pp. 159–166.
[58] P. Ren, M. Tao, A decentralized sleep mechanism in heterogeneous cellular networks with QoS constraints, IEEE Wirel. Commun. Lett. 3 (5) (2014) 509–512.
[59] L. Li, W. Meng, Collaborative base station sleeping solution design in heterogeneous cellular network, in: 2022 27th Asia Pacific Conference on Communications, APCC, IEEE, 2022, pp. 231–235.

Greta Vallero is a researcher at the department of Electronics and Telecommunication of the Politecnico di Torino. She obtained her master's degree in ICT for Smart Societies (Telecommunication Engineering), in October 2017 and her PhD in 2022, presenting the thesis entitled "Green Mobile Networks: from 4G to 5G and Beyond". Her main research interests are the energy efficiency and resilience of Radio Access Networks, using the support of Machine Learning algorithms, the design of infrastructure management approaches and the employment of renewable energy supply, also considering the new technologies and paradigms introduced with 5G and 6G networks, such as Multi-Access Edge Computing, drones and High Altitude Platform Stations.

Michela Meo Michela Meo received the Laurea degree in electronic engineering and the Ph.D. degree in electronic and telecommunications engineering from the Politecnico di Torino, Italy, in 1993 and 1997, respectively, where she has been a Professor since 2006. She has co-authored about 200 papers and edited a book with Wiley and special issues of international journals, including ACM Monet, Performance Evaluation, and Computer Networks. Her research interests include performance evaluation and modeling, green networking, and traffic classification and characterization. She is an Associate Editor of the IEEE Communications Surveys & Tutorials and an Area Editor of the IEEE Transactions on Green Communications and Networking. He was an Associate Editor of the IEEE Transactions of Networking. She chairs the Steering Committee of IEEE OnlineGreenComm and the International Advisory Council of ITC. She was the Program Co-Chair of several conferences, including ACM MSWiM, IEEE Online GreenComm, IEEE ISCC, IEEE Infocom Miniconference, and ITC.

Wout Joseph received the M. Sc. degree in electrical engineering from Ghent University (Belgium) in July 2000. From September 2000 to March 2005, he was a research assistant at the Department of Information Technology (INTEC) of the same university. During this period, his scientific work was focused on electromagnetic exposure assessment. His research work dealt with measuring and modeling of electromagnetic fields around base stations for mobile communications related to the health effects of the exposure to electromagnetic radiation. This work led to a Ph.D. degree in March 2005. Since April 2005, he has been a postdoctoral researcher for IBBT-Ugent/INTEC (Interdisciplinary institute for BroadBand Technology). Since October 2007, he has been a Post-Doctoral Fellow of the FWO-V (Research Foundation – Flanders). Since October 2009 he has been a professor in the domain of "Experimental Characterization of wireless communication systems." His professional interests are electromagnetic field exposure assessment, propagation for wireless communication systems, antennas and calibration. Furthermore, he specializes in wireless performance analysis and Quality of Experience.

Margot Deruyck received the M. Sc. degree in Computer Science Engineering and the Ph.D. degree from Ghent University, Ghent, Belgium, in 2009 and 2015, respectively. From September 2009 to January 2015, she was a Research Assistant with Ghent University IMEC – WAVES (Wireless, Acoustics, Environment & Expert Systems – Department of Information Technology). Her scientific work is focused on green wireless access networks with minimal power consumption and minimal exposure from human beings. This work led to the Ph.D. degree. Since January 2015, she has been a Postdoctoral Researcher at the same institution where she continues her work in green wireless access networks.